Theory of spin polarization in the metastable-He–metal interaction

L. A. Salmi
Institute of Theoretical Physics, Chalmers University of Technology, S-412 96 Göteborg, Sweden
(Received 3 February 1992)

In a recent experiment by Hart *et al.*, the spin polarization of electrons emitted in the interaction between metastable He and Cu was measured as a function of their kinetic energy. The polarization was found to increase with increasing electron energy from approximately 22% at the lowest energy to around 75% at the highest energy. The purpose of the present work is to show the crucial role played by three factors: the exchange interaction in Auger neutralization, secondary electrons, and Auger deexcitation. With these, we explain why there is a measured spin polarization and why the spin polarization increases with increasing kinetic energy of the ejected electrons. Using a simple model for the copper wave functions and including surface screening, our calculation shows a good agreement with the experimental results.

I. INTRODUCTION

There has been increasing interest in the spin dependence of electron scattering from surfaces,[1–4] especially since it has the potential for obtaining information about the exchange scattering. Recent experiments utilize a spin-polarized beam as well as spin detection of the scattered electrons to obtain information about different scattering channels in magnetic materials.[5] However, in those experiments the number of scattered electrons in different channels includes effects from the difference in occupation of spin-up and spin-down electron states *and* the exchange process. To *isolate the effect of exchange,* which is a property already of the nonmagnetic solid, spin-polarized metastable-atom-deexcitation spectroscopy (SPMDS) on *nonmagnetic materials* will be shown in this work to yield important information to this point. We are particularly interested in the He-Cu system.[6,7] The He-metal (or H-metal) interaction has been studied by various authors,[8–10]—though without focusing specifically on the exchange effect. The purpose of this work is therefore to go beyond those treatments by focusing strongly on the exchange effect itself and to show how the result of a SPMDS experiment on a nonmagnetic material, such as Cu,[6] directly measures the exchange scattering.

The spin polarization of electrons emitted when a thermal-energy beam of metastable He(2^3S) atoms is deexcited at a clean Cu(100) surface was recently measured.[6] Figure 1 shows the experimental cross section (small dots) and spin polarization as a function of the kinetic energy of the ejected electrons. The incident excited helium atoms can undergo an Auger deexcitation process, where one metal electron makes a transition into the empty He 1*s* state (see Fig. 2). Energy is transferred to the excited He 2*s* electron, which then can leave the atom. Since the copper work function is sufficiently large, there is a competing process where the incident metastable He atom also can undergo resonant ionization. The resulting He^+ ion continues toward the surface and is quickly neutralized by a metal conduction electron, and the resulting Auger electron can be ejected if it has enough energy to surmount the surface barrier. From the work by Hagstrum, we know that there is a most probable distance where the neutralization process takes place.[8] For a thermal beam of helium this distance is approximately 2 Å. The electrons produced in the Auger neutralization process can also cause a cascade of secondary electrons, produced from electron-electron col-

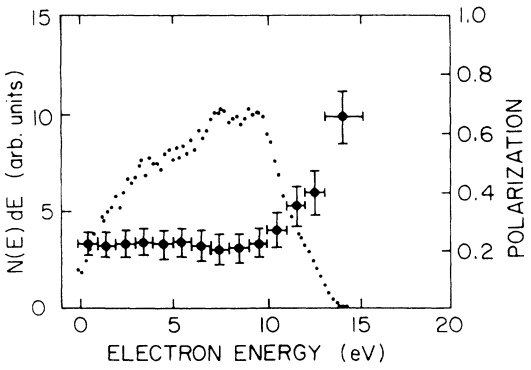

FIG. 1. Experimentally determined electron energy distribution (●) and polarization (+) for metastable He(2^3S) deexcitation at a clean Cu(100) surface (Ref. 6).

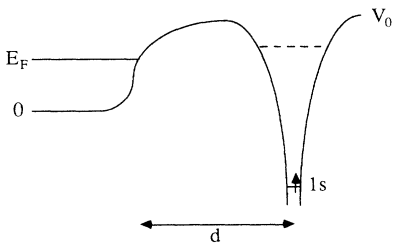

FIG. 2. Potential-energy diagram of a He^+ ion at a distance d from a metal surface. E_F and V_0 are the Fermi and vacuum energy levels. 1*s* represents the He ground state and the energy zero is put at the bottom of the conduction band. The empty He 2*s* state is indicated with a dashed line.

lisions, which yields a third contribution to the measured yield.

In Sec. II we treat the production of electrons from the Auger neutralization process. Starting from the golden rule, we derive expressions for the production rate and the spin polarization, which we calculate numerically. In this calculation we include an exchange matrix element, use approximate wave functions from the square barrier model, and include a scheme for frequency and wave-vector-dependent dynamical surface screening.

Section III contains the calculation of secondary electrons. Using a simple model, we calculate the contribution of secondary electrons to both the total production rate and the spin polarization.

Auger deexcitation and resonant ionization rates are estimated in Sec. IV. Using the same ingredients as in the Auger neutralization process, we calculate the contribution to the production rate and the spin polarization. The importance of the different processes at different distances between the atom/ion and the surface is discussed in Sec. V. From this we conclude that the processes can be characterized by a most probable distance, where they take place. A summary and conclusions ends the paper in Sec. VI.

Altogether, the Auger neutralization, secondary electrons, and Auger deexcitation explain the experimentally observed cross section and spin polarization in metastable He and Cu interaction.

II. AUGER NEUTRALIZATION

In this section, we start from the golden-rule transition probability and develop the theory for the Auger neutralization (AN) process. The theory incorporates an exchange matrix element and dynamical metal screening. Production rates and spin polarization are calculated numerically for different selected distances between the ion and the surface. We then choose the most probable distance as a representative distance of the process, to compare with the experimental measurements.

Consider a spin-polarized He^+ ion at a distance d from a metal surface as in Fig. 2. In our calculation we use a Fermi energy of 9 eV that corresponds to electron band calculations.[11] V_0 is the vacuum level, and the helium ground state $|1s\rangle$ at infinite distance from the surface is set to be 24.6 eV below the vacuum level. A metal electron can neutralize the ground state of the He^+ ion. Since the He^+ ion is 100% spin polarized (with spin up for convenience) this electron can only have a spin opposite to the He^+ electron. However, the emitted Auger electron can have both spin up or down but with different probabilities. This is the basic reason for measuring a finite polarization of the outgoing Auger electrons. If the detected electron has spin up there is only one possible process [Fig. 3(a)], but if the emitted electron is detected with spin down there are two different possible processes between specific initial and final states [Fig. 3(b)]. One is as the direct process, and the other (dashed) is the exchange process.

From the golden rule, we write the transition probabilities per unit time and per energy interval for the emission

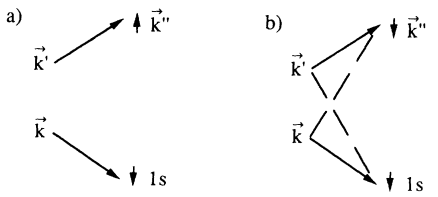

FIG. 3. Auger neutralization. (a) shows the emission of spin-up electrons $N_\uparrow(E)$ and (b) the emission of spin-down electrons $N_\downarrow(E)$. The full lines are the direct and the dashed lines are the exchange neutralization processes. The ejected electron is denoted $\mathbf{k}''$, the empty He ground-state hole $1s$, and $\mathbf{k}$ and $\mathbf{k}'$ are metal conduction-band electrons.

of spin-up and spin-down electrons detected at an energy E as

$$N_\uparrow(E)=\frac{2\pi}{\hbar}\sum_{\mathbf{k},\mathbf{k}',\mathbf{k}''} f(k)f(k')[1-f(k'')] \times|M^{\mathbf{k}\mathbf{k}'}_{1s\mathbf{k}''}|^2\delta(E_{\mathbf{k}''}-E_{\mathbf{k}'}+E_{1s}-E_{\mathbf{k}}) \times\delta(E_{\mathbf{k}''}-E)\ , \tag{1}$$

$$N_\downarrow(E)=\frac{2\pi}{\hbar}\sum_{\mathbf{k},\mathbf{k}',\mathbf{k}''} f(k)f(k')[1-f(k'')] \times\tfrac{1}{2}|M^{\mathbf{k}\mathbf{k}'}_{1s\mathbf{k}''}-M^{\mathbf{k}'\mathbf{k}}_{1s\mathbf{k}''}|^2 \times\delta(E_{\mathbf{k}''}-E_{\mathbf{k}'}+E_{1s}-E_{\mathbf{k}})\delta(E_{\mathbf{k}''}-E)\ , \tag{2}$$

where f is the $T=0$ Fermi factor and M the Coulomb interaction matrix element. $|\mathbf{k}\rangle$ and $|\mathbf{k}'\rangle$ are both metal conduction-electron states, $|\mathbf{k}''\rangle$ is a free-electron state, and $|1s\rangle$ is the helium electron ground state. In the expression for $N_\downarrow(E)$, exchange effects are taken into account by the standard antisymmetrization of the matrix element, where the factor $\frac{1}{2}$ ensures that we get zero polarization if we neglect interference between matrix elements.

In the experiment by Hart *et al.*,[6] the polarization of the Auger electron yield is defined as

$$P(E)=\frac{N_\uparrow(E)-N_\downarrow(E)}{N_\uparrow(E)+N_\downarrow(E)}\equiv\frac{A}{B-A}\ , \tag{3}$$

where $N_\uparrow(E)$ and $N_\downarrow(E)$ are the number of spin-up and spin-down Auger electrons, as described above in Eqs. (1) and (2). Without exchange effects the measured polarization would be zero, which is not in accordance with the experimental findings of Ref. 6. The quantities A and B introduced in Eq. (3) can be expressed, using Eqs. (1) and (2), as

$$A=\frac{2\pi}{\hbar}\sum_{\mathbf{k},\mathbf{k}',\mathbf{k}''} f(k)f(k')[1-f(k'')]\mathrm{Re}\{M^{\mathbf{k}\mathbf{k}'}_{1s\mathbf{k}''}M^{\mathbf{k}'\mathbf{k}*}_{1s\mathbf{k}''}\} \times\delta(E_{\mathbf{k}''}-E_{\mathbf{k}'}+E_{1s}-E_{\mathbf{k}})\delta(E_{\mathbf{k}''}-E)\ , \tag{4}$$

$$B=\frac{2\pi}{\hbar}\sum_{\mathbf{k},\mathbf{k}',\mathbf{k}''} f(k)f(k')[1-f(k'')]2|M_{1s\mathbf{k}''}^{\mathbf{k}\mathbf{k}'}|^2 \times\delta(E_{\mathbf{k}''}-E_{\mathbf{k}'}+E_{1s}-E_{\mathbf{k}})\delta(E_{\mathbf{k}''}-E)\ , \quad (5)$$

where M is the Coulomb matrix element. If we neglect exchange, we observe that $A\equiv 0$ and $P\equiv 0$. Taking the Fourier transform of the Coulomb interaction in the parallel direction, assuming translational invariance of the copper surface, and using the classical surface response function (see, e.g., Ref. 12), the matrix element can be expressed as

$$M_{1s\mathbf{k}''}^{\mathbf{k}\mathbf{k}'}=\frac{2\pi}{L^2}\frac{e^2}{4\pi\epsilon_0}\sum_{\mathbf{q}_\parallel}\frac{1}{q_\parallel}\langle 1s(\mathbf{x}_1)\mathbf{k}''(x_2)|\left[\frac{2}{\epsilon(\omega)+1}e^{-q_\parallel|z_2-z_1|}[1-\Theta(z_2)] + \left[e^{-q_\parallel|z_2-z_1|}-\frac{\epsilon(\omega)-1}{\epsilon(\omega)+1}e^{-q_\parallel|z_2+z_1|}\right]\Theta(z_2)\right]e^{i\mathbf{q}_\parallel\cdot(\mathbf{x}_{2\parallel}-\mathbf{x}_{1\parallel})}|\mathbf{k}(\mathbf{x}_1)\mathbf{k}'(\mathbf{x}_2)\rangle\ , \quad (6)$$

where $\omega\equiv E_{\mathbf{k}''}-E_{\mathbf{k}'}=E_{\mathbf{k}}-E_{1s}$ is the energy transfer and Θ is a unit-step function. Here $z=0$ corresponds to the square barrier step in the electron potential at the metal surface and the metal is in the $z<0$ region. Since the classical response function contains $\epsilon(\omega)$, it describes the dynamical screening of the neutralization event by the metal. We consider this to be an important piece of physics to include, and in this sense our treatment goes beyond Refs. 7–10. However, then we are not fully treating the spatial screening of the external potential. To find a remedy for this, we later introduced a $k_\parallel$-dependent so-called surface dielectric function.

The expression for the matrix element can be simplified if it can be separated with respect to the perpendicular coordinates z_1 and z_2 of the electronic wave functions. To investigate if such a separation is a valid approximation, we need to look more carefully at the following integral:

$$\langle 1s(z_1)|e^{-q_\parallel|z_2-z_1|}|\mathbf{k}(z_1)\rangle=\int_{-\infty}^{z_2}dz_1\,\phi_{1s}^*(z_1)e^{-q_\parallel(z_2-z_1)}\phi_{k_\perp}(z_1)+\int_{z_2}^{\infty}dz_1\,\phi_{1s}^*(z_1)e^{-q_\parallel(z_1-z_2)}\phi_{k_\perp}(z_1)\equiv I_1+I_2\ . \quad (7)$$

If the first integral I_1 is negligible compared to I_2, i.e., $I_1/I_2\ll 1$, a separation is valid. A closer look at I_1 and I_2 gives at hand that $I_1/I_2<0.1$ for $z_2/d<0.5$, where d is the ion-surface separation and z_2 is the perpendicular coordinate of $|\mathbf{k}'\rangle$ and $|\mathbf{k}''\rangle$. When z_2 is close to the distance d between the surface and the He^+ ion, $I_1/I_2\approx 1$, and the approximation is no longer valid. On the other hand, the metal electron state $|\mathbf{k}''(\mathbf{x}_2)\rangle$ decays exponentially outside the surface and gives negligible contribution to the integral over z_2. The separation is therefore a reasonable approximation. After the separation of the matrix element with respect to the coordinates z_1 and z_2, as described above, the matrix element in Eq. (6) can be written as

$$M_{1s\mathbf{k}''}^{\mathbf{k}\mathbf{k}'}=\frac{2\pi}{L^2}\frac{e^2}{4\pi\epsilon_0}\sum_{\mathbf{q}_\parallel}\frac{1}{q_\parallel}\langle 1s(\mathbf{x}_1)|e^{-i\mathbf{q}_\parallel\cdot\mathbf{x}_{1\parallel}}e^{-q_\parallel z_1}|\mathbf{k}(\mathbf{x}_1)\rangle \times\langle\mathbf{k}''(\mathbf{x}_2)|\left[\frac{2}{\epsilon(\omega)+1}e^{q_\parallel z_2}[1-\Theta(z_2)]+\left[e^{q_\parallel z_2}-\frac{\epsilon(\omega)-1}{\epsilon(\omega)+1}e^{-q_\parallel z_2}\right]\Theta(z_2)e^{i\mathbf{q}_\parallel\cdot\mathbf{x}_{2\parallel}}\right]|\mathbf{k}'(\mathbf{x}_2)\rangle\ . \quad (8)$$

To be able to calculate the matrix element further, we need to specify appropriate wave functions. For the metal conduction-electron states $|\mathbf{k}\rangle$ and $|\mathbf{k}'\rangle$ we use free-electron states calculated from a jellium model with a square barrier confining potential. In our calculation we use $z=0$ as the position of the potential step and for the position of the image plane. This means that we use different screening functions for $z_2>0$ and $z_2<0$, as seen in Eq. (6). In general, the position of the image plane depends on frequency, but a frequency-independent choice is a rather good one for low and intermediate frequencies compared to the plasma frequency of the metal.[12] This is certainly better than using the classical image plane that is at the jellium edge. Our wave functions describe s-band states in a reasonable way, but fail to give any information about the d-band states of copper. However, d-band states give, as argued below, a negligible contribution to the AN process. Therefore, assuming translational invariance parallel to the surface, and using box normalization (size L), these wave functions can be written in the form[13]

$$\psi_{\mathbf{k}}(\mathbf{x})=\frac{1}{L}e^{i\mathbf{k}_\parallel\cdot\mathbf{x}_\parallel}\phi_{k_\perp}(z),\quad E_k<E_F\ , \quad (9)$$

where the perpendicular part is

$$\phi_{k_\perp}(z)=\frac{1}{\sqrt{L}}(e^{ik_\perp z}+r_k e^{-ik_\perp z})[1-\Theta(z)] + \frac{1}{\sqrt{L}}t_\kappa e^{-\kappa z}\Theta(z) \quad (10)$$

and the transmission and reflection coefficients are

$$t_k=\frac{2k_\perp}{k_\perp+i\kappa}\ , \quad (11)$$

$$r_k=\frac{k_\perp-i\kappa}{k_\perp+i\kappa}\ , \quad (12)$$

with the decay constant κ given by

$$\kappa^2=\frac{2mV_0}{\hbar^2}-k_\perp^2 \ . \tag{13}$$

The free-electron state $|\mathbf{k}''\rangle$ is taken as a plane wave corresponding to Eqs. (9) and (10), but with $E_{k''}>E_F$. Outside a metal surface, the magnitudes of the wave functions decrease the more localized the orbitals are. Of particular importance in the AN process is the magnitude of the metal wave function at the position of the He ion. Because of this, and the fact that the ejected Auger electrons originate from the surface region, the contribution from d electrons in the measured Auger spectrum is very small.[14,15]

The hydrogenlike helium $1s$ ground state in the ion is described by an exponentially decaying orbital with decay constant λ_{1s}. λ_{1s} is set to 1.69 a_0^{-1}, which is the value given by a variational calculation of the helium atom.[13] The helium core is at the distance d outside the metal surface. In the following calculations, we use the approximation of treating the $1s$ state as strongly localized at the position of the helium ion. Integrals involving the $1s$ wave function therefore reduce to integrals over only the $1s$ wave function, a quantity that we define as $V_{1s}^{1/2}$ with $V_{1s}=64\pi/(\lambda_{1s})^3$. The rest of the integrand is evaluated at the point $z=d$.

An exponentially decaying orbital describes the $1s$ state well when the helium ion is far outside the metal surface. In approaching the metal surface we expect the energy level to move up.[16] We use the classical image shift $e^2/(16\pi\epsilon_0 z)$ as an approximation of this increase in energy as the helium approaches the surface. This should of course be more accurate for large distances outside the surface. At closer distances we know that hybridization and reorientation of orbitals may alter the energy level in a manner different from the classical image shift.[17] However, this is most important for more extended wave functions, i.e., for excited helium states.

Putting everything together we now express A and B, defined in Eqs. (3)–(5), as

$$A=\frac{2\pi}{\hbar}\left[\frac{e^2}{4\pi\epsilon_0}\frac{2\pi}{L^3}\right]^2 V_{1s}\sum_{\mathbf{k},\mathbf{k}',\mathbf{k}''} f(k)f(k')[1-f(k'')]\frac{1}{|\mathbf{k}_\parallel''-\mathbf{k}_\parallel'|\,|\mathbf{k}_\parallel''-\mathbf{k}_\parallel|}e^{-(|\mathbf{k}_\parallel''-\mathbf{k}_\parallel'|+|\mathbf{k}_\parallel''-\mathbf{k}_\parallel|)d}$$
$$\times\mathrm{Re}\{N(k_\perp'',k_\perp',|\mathbf{k}_\parallel''-\mathbf{k}_\parallel'|,\omega)\phi_{k_\perp}(d)N^*(k_\perp'',k_\perp,|\mathbf{k}_\parallel''-\mathbf{k}_\parallel|,\omega')\phi_{k_\perp'}^*(d)\}$$
$$\times\delta(\omega+E_{1s}-E_{\mathbf{k}})\delta(E_{\mathbf{k}''}-E) \ , \tag{14}$$

$$B=\frac{2\pi}{\hbar}\left[\frac{e^2}{4\pi\epsilon_0}\frac{2\pi}{L^3}\right]^2 V_{1s}\sum_{\mathbf{k},\mathbf{k}',\mathbf{k}''} f(k)f(k')[1-f(k'')]\frac{2}{|\mathbf{k}_\parallel''-\mathbf{k}_\parallel'|^2}e^{-2|\mathbf{k}_\parallel''-\mathbf{k}_\parallel'|d}$$
$$\times|N(k_\perp'',k_\perp',|\mathbf{k}_\parallel''-\mathbf{k}_\parallel'|,\omega)\phi_{k_\perp}(d)|^2\delta(\omega+E_{1s}-E_{\mathbf{k}})\delta(E_{\mathbf{k}''}-E) \ , \tag{15}$$

where N is defined as

$$N(k_\perp'',k_\perp',q_\parallel,\omega)=\int_{-\infty}^{0}dz_2\phi_{k_\perp''}^*(z_2)\frac{2}{\epsilon(\omega)+1}e^{q_\parallel z_2}\phi_{k_\perp'}(z_2)+\int_0^\infty dz_2\phi_{k_\perp''}^*(z_2)\left[e^{q_\parallel z_2}-\frac{\epsilon(\omega)-1}{\epsilon(\omega)+1}e^{-q_\parallel z_2}\right]\phi_{k_\perp'}(z_2) \ . \tag{16}$$

With wave functions according to Eqs. (9)–(13), N can be solved analytically. Due to the exponentially decaying wave functions, the integral can be neglected in the $\pm\infty$ limits. However, it turns out that it is crucial not to neglect the integral in the region between the surface and the helium ion.

In the expression for the matrix element in Eq. (8), we recognize $q_\parallel$ in the denominator as caused by the long-range Coulomb interaction. Nevertheless, the sum over $q_\parallel$ does not diverge for $q_\parallel\to 0$, because the wave functions are orthogonal. Normally this is solved by a proper orthogonalization of the wave functions. Neglecting the orthogonalization will result in an overestimate of the transition rates. Here we use a different method than usual by introducing a lower cutoff in momentum space. This is done by adding a factor to $q_\parallel$ in the nominator of Eq. (8) such that $q_\parallel\to q_\parallel+1/d^*$. The length d^* given by Eq. (17) below ensures that we get the correct finite limit when $q_\parallel\to 0$.

$$d^*=\frac{\langle 1s|z|\mathbf{k}\rangle}{\langle 1s|\mathbf{k}\rangle} \ . \tag{17}$$

Evaluating d^* in Eq. (17) with the wave functions described above gives $d^*=d$.

The dynamical response of the metal to the rapid neutralization process is contained in the surface response function in Eq. (8). This is a classical response function in the sense that it contains only an ω dependence. Spatial screening is neglected in this purely classical model. However, we know that the correct screening also exhibits spatial screening. This is traditionally done within the Thomas-Fermi model, which in turn implies neglecting all dynamical screening effects.[18] To introduce an ω- and $k_\parallel$-dependent screening, we proceed as described in Appendix A by substituting $\epsilon(\omega)$ for the so-called surface response function $\epsilon(\mathbf{k}_\parallel,\omega)$ according to

$$\frac{1}{\epsilon(\omega)}\to\frac{1}{\epsilon(\mathbf{k}_\parallel,\omega)}\equiv\frac{k_\parallel}{\pi}\int\frac{dk_\perp}{k_\parallel^2+k_\perp^2}\frac{1}{\epsilon(\mathbf{k}_\parallel,k_\perp,\omega)} \ . \tag{18}$$

$\epsilon(\mathbf{k}_\parallel,k_\perp,\omega)$ is for convenience taken from the hydrodynamic approximation:[18]

$$\epsilon(\mathbf{k}_\parallel, k_\perp, \omega) = 1 - \frac{\omega_p^2}{\omega^2 - \beta^2(k_\parallel^2 + k_\perp^2)} , \tag{19}$$

where ω_p is the plasma frequency, $\beta = 0.77 v_F$, and v_F is the Fermi velocity. Setting Eq. (19) into Eq. (18) yields

$$\frac{1}{\epsilon(\mathbf{k}_\parallel, \omega)} = \frac{1}{\epsilon(\omega)} \left[1 + \frac{\epsilon(\omega) - 1}{\left[1 + \frac{1}{Y^2(k_\parallel)} \frac{\epsilon(\omega)}{\epsilon(\omega) - 1} \right]^{1/2}} \right] , \tag{20}$$

where Y is defined as

$$Y(k_\parallel) = \frac{k_\parallel \beta}{\omega_p} . \tag{21}$$

We notice that Eq. (20) exhibits the correct limit when $\beta \to 0$, since the right-hand side of Eq. (20) reduces to $1/\epsilon(\omega)$ as expected. For $\epsilon(\omega)$, we now use the dielectric function for copper taken from experimental measurements.[19] Thereby d electrons are included in the screening, which is important inside the solid.

Taking everything together, we first calculate the total internal *energy-integrated* Auger rate at different distances for the helium ion outside the metal surface as shown in Fig. 4. This figure also contains the rates for the Auger deexcitation (AD) and resonant ionization (RI) processes, as discussed in Sec. IV below. Technically, the integrations are performed by using the Monte Carlo integration method. We notice that the curves exhibit a slight convex behavior, which was predicted earlier.[20] Using square barrier wave functions for the metal states has earlier been shown to yield production rates that are lower than when using more accurate metal wave functions.[7] However, screening increases the production rates slightly. This phenomenon can be explained by studying the values of the dielectric function for copper in the appropriate energy range. Because screening typically comes in as a factor $1/\epsilon$, we expect higher production rates whenever $|\mathrm{Re}(\epsilon)| < 1$, a condition of antiscreening, which is fulfilled in our case. The AD and RI rates are much larger than the AN rate for specific distances outside the surface. We notice a stronger dependence on the distance, i.e., a steeper slope, for the AN rate. This has its origin in the AN matrix element in Eq. (8), which contains two metal states, whereas the AD and RI matrix elements only contain one metal state, as shown below in Eqs. (25) and (26).

The ejected electron rate from AN *per unit energy interval* for a fixed distance between the helium ion and the metal surface is calculated using the same method as above. For a distance of 3 Å this gives the result shown in Fig. 5. The choice of $d = 3$ Å is based on the best fit of our calculation to the experimental polarization. Although the absolute magnitude of the rate in Fig. 5 depends strongly on the distance d, the shape does not. The curve gets its main shape from the convolution of free-electron densities of states. This has to do with the fact that matrix element effects on the *total* rates are weak compared to the influence from a limited momentum space.

The polarization exhibits a strong dependence on the distance d since the polarization involves a difference between matrix elements. Figure 6 shows the polarization of the ejected electron distribution for various distances outside the surface. We notice that the polarization is near 100% at the lowest energies. This strong polarization is partly a result of the surface barrier. Because the angular distributions of spin-up and spin-down electrons inside the solid are not equal, the surface acts like a filter that favors the transmission of spin-up electrons. For $d = 3$ Å, we get a polarization of approximately 20–40 % in the middle-energy range. Later we will show that taking secondary electrons into account gives for $d = 3$ Å a polarization of around 20% in both the low- and middle-energy ranges, which corresponds to the experimental values. A more elaborate calculation should also average

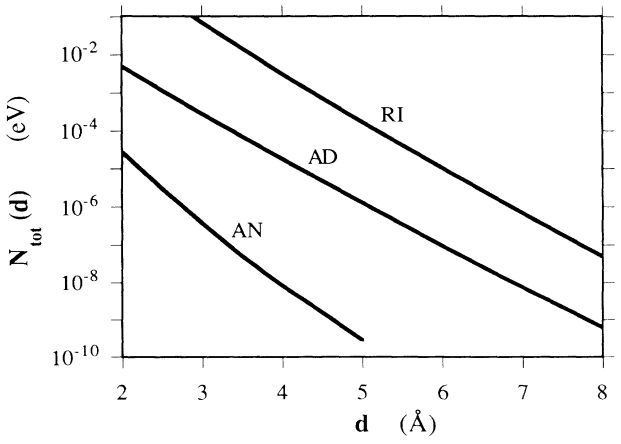

FIG. 4. Calculated total-energy integrated Auger neutralization rate $N_{tot} = N_\uparrow + N_\downarrow$, expressed in eV as a function of the distance d between the helium ion and the metal surface. Also indicated in the figure are the Auger-deexcitation and resonant ionization rates, which are treated in Secs. III and IV.

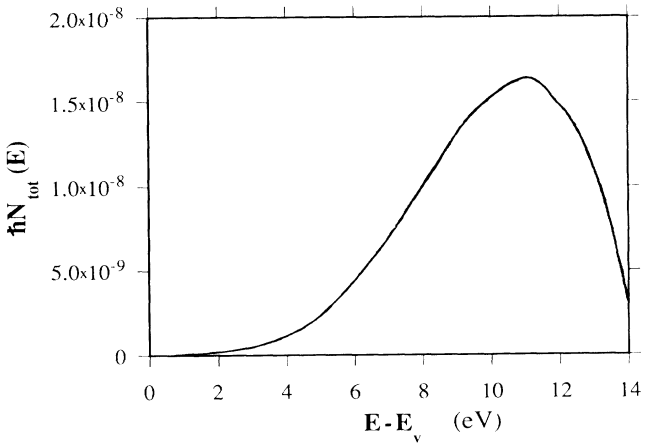

FIG. 5. Calculated total ejected electron distribution per unit energy interval, $N_{tot}(E) = N_\uparrow(E) + N_\downarrow(E)$, from the Auger neutralization process at a distance of 3 Å between the helium ion and the metal surface. E_v is the vacuum level.

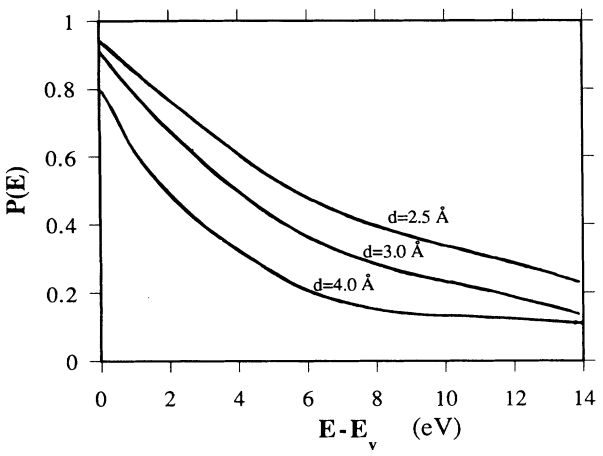

FIG. 6. Polarization $P(E)$ of ejected electrons produced in the Auger neutralization process as a function of ejected electron kinetic energy. The polarization has been calculated for different distances d (2.5, 3.0, and 4.0 Å) between the helium ion and the metal surface. E_v is the vacuum level.

over the ion-surface distance of the He trajectory. Instead we use the most probable distance as a representation of the whole continuous sequence of processes as discussed and motivated below in Sec. V.

For lower energies, the theory of AN cannot explain either the experimental cross section or the spin polarization as shown in Fig. 1. This leads us to consider other possible processes. We later show that the lower-energy part of the curves can be explained by incorporating secondary electrons emitted by the Auger electrons, as proposed recently.[17] Because secondary electrons are preferably produced at lower energies, the rate in Fig. 5 is expected to increase and the spin polarization to decrease for lower energies if we incorporate secondary electrons in our calculations. There is also a disagreement in the highest-energy range between our theory and the experimental results. This is particularly obvious in the polarization diagram. We suggest below that the AD process is of importance at these high energies. This is in accordance with the recent predictions that excited helium can survive quite close to the metal surface and therefore AD can compete effectively with the RI and AN processes.[17]

In this section we have calculated the production rates and the polarization for the AN process. We note that the nonzero polarization originates from the exchange matrix element. However, the disagreement between the theoretical and experimental curves leads us to take a closer look at other possible processes in He-metal interaction. We start in the next section by considering secondary electrons.

III. SECONDARY ELECTRONS

We found in the preceding section that we could not account for the experiment at low kinetic energies. A reason for this can be that we have neglected the production of secondary electrons. Using a simple model, we show in this section that the ejected electrons from the metastable He-metal interaction produce a cascade of secondary electrons that are mainly produced in the lower energy region. This secondary-electron cascade explains both the rate and the polarization of the ejected electrons at low energies, as measured experimentally.

Secondary-electron cascades have earlier been described successfully by starting with the Boltzmann transport equation.[21] A spherical average of this transport equation can be written as[22]

$$N(E)=S(E)+\int_E^\infty dE'F(E',E)N(E') , \tag{22}$$

where S is the primary electron distribution, N is the secondary-electron distribution, and F is the scattering kernel, giving the probability per unit energy of an electron at E' being scattered to E. Here S is the internally produced electron distribution from the AN process. Because every primary electron produces two secondary electrons in a collision, a sum rule for secondary electrons can be deduced. We use, assuming that the sum rule has a strong influence of the secondary-electron production, a simple approximation for the kernel in the transport equation that fulfills the sum rule,[22]

$$F(E',E)=\frac{2}{E'-E_F} . \tag{23}$$

This approximation has earlier been shown to give a good approximation to more elaborate calculations, particularly for higher secondary-electron energies.[22] For energies close to the Fermi level, Eq. (23) diverges and obviously gives too high a secondary production rate. In our case we do not have to calculate secondary electrons close to the Fermi level, since the metal work function inhibits those electrons from escaping from the solid.

Equations (22) and (23) give the secondary-electron distribution before escaping the surface. To calculate the ejected secondary-electron distribution, we need a surface transmission function. It has earlier been concluded that the probability to escape the surface does not depend strongly on the type of ion, and that the final state density is a relatively smooth function of the energy.[14] Different escape probability functions have been used, but they differ little from each other for energies larger than 4 eV above the vacuum level.[14] Because of this, and the fact that we expect the secondary electrons to exhibit an angular dependence similar to the AN distribution, we use a surface transmission function $P(E)$ that is the ratio of the calculated ejected and internal AN distribution.

In bulk, Eq. (22) should be iterated to give all orders of secondary processes. In the surface region, where the AN takes place, we cannot assume infinite orders of the secondary process. Mean free paths in this energy region have been calculated to be in the order of 5–10 Å.[23] Therefore we expect only the first few orders of secondary electrons to be important, since they have a high probability to reach and escape the surface without further interacting through higher-order secondary processes. We also notice that the mean free path increases with decreasing electron energy in this particular energy region.[23] This suggests that most of the secondary electrons generated moving toward the surface, within the surface region, will escape the surface and therefore in-

hibit higher orders of secondary-electron generation. Based on these ideas, we do an approximation where all Auger electrons produced in a direction toward the surface escape according to the surface transmission function $P(E)$ without generating any secondary electrons. Auger electrons that are unable to escape are assumed to generate the first generation of secondary electrons. Because we use a spherical average for the secondary-electron production, we assume for simplicity that the secondary electrons are also escaping the solid according to the transmission function $P(E)$. The fraction of the first generation of secondary electrons that do not escape the surface generates a second generation of secondary electrons, etc.

Within these approximations, we calculate the ejected electron distribution of the AN process with associated secondary-electron cascade for the selected ion-surface distance of $d=3$ Å. This gives a polarization of around 20%, as shown (dashed) in Fig. 7. The secondary electrons give higher production rates in the low-energy range with a curvature that gives a good agreement with the experimental result. Given the source distribution $S(E)$, i.e., the internal Auger distribution, we note that Eq. (22) gives the absolute number of secondary electrons and therefore the strength of the total distribution $N(E)$ of Auger *and* secondary electrons without adjustable parameters. To get an amount of secondary electrons that agrees with the measurement, we have to incorporate at least two generations of secondary electrons. Higher orders of secondary-electron generations give only a negligible contribution to the ejected electron rate in Fig. 7.

Ignoring spin-flip scattering, each secondary-electron process will create two secondary electrons with no preferable spin direction. A source distribution of electrons with high polarization, which is the case for the AN electrons at low energies (see Fig. 6), will therefore be diluted with electrons of zero average polarization. This results in a decrease of the total polarization. From Fig. 7, we observe a clear decrease in polarization to approximately 20% in the low-energy range. The resulting, almost energy-independent, polarization corresponds well to the experimental measurement in Fig. 1 for kinetic energies up to 10 eV.

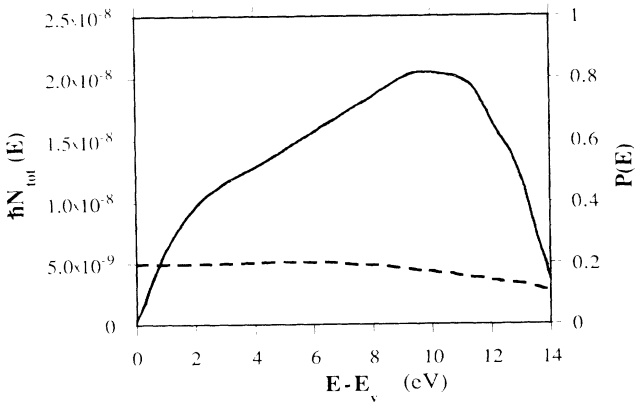

FIG. 7. Calculated total ejected electron distribution per energy interval $N_{\rm tot}(E)=N_{\uparrow}(E)+N_{\downarrow}(E)$, and spin polarization $P(E)$ (dashed line) as a function of ejected electron energy from the Auger neutralization and secondary-electron processes. The calculation is done for a distance of 3 Å between the helium ion and the metal surface. E_v is the vacuum level.

Using a simple theory, we have approximated the secondary-electron contribution to the AN process. Clearly, secondary electrons can explain the high production rates at lower energies. Also, the relatively energy-independent polarization at lower energies can be explained as an effect of secondary electrons. There is, however, still a disagreement between theory and experiment for the highest energies. In the next section we therefore consider the Auger-deexcitation process as a possible cause of this.

IV. AUGER DEEXCITATION AND RESONANT IONIZATION

In this section, we discuss the Auger deexcitation (AD) and resonant ionization (RI) processes. Using the same ingredients as above, we estimate the rates for different selected distances between the excited atom and the surface. Our calculation shows that the AD process *is* important in the high-energy region, and explains the experimentally observed increase in polarization for high energies.

For the AD process we start with metastable helium atoms instead of ions far outside the surface. At large atom-surface distances the excited state, here labeled $|2s\rangle$, lies below the Fermi level of the metal. In approaching the surface the excited state increases in energy, classically expressed by the image shift as described above. For a certain distance the excited electron is in line with the Fermi level and has the possibility to tunnel into the metal. We are then left with a helium ion and the possibility of AN to occur as described in Sec. II. Before tunneling, however, there is a possibility for the AD process to take place. The situation with a metastable atom outside the metal surface is shown in Fig. 8. Ignoring the effect of p orbitals, we let the energy level of the isolated excited $2s$ state be 4.8 eV below the vacuum level. For copper, the work function is 4.55 eV. The possible AD process is illustrated in Fig. 9.

Obviously the polarization from the AD process is always 100%, since there are no escaping electrons with spin down. The production rates per time and per energy interval can be expressed from the golden rule in the

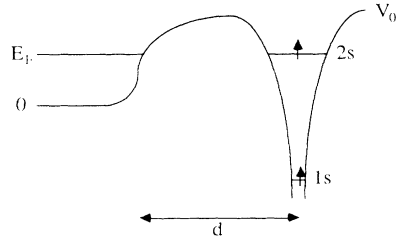

FIG. 8. Potential-energy diagram of an excited spin-polarized He atom at a distance d from a metal surface. E_F and V_0 are the Fermi and vacuum energy levels. $1s$ represents the He ground state, $2s$ the excited He state, and the energy zero is put at the bottom of the conduction band.

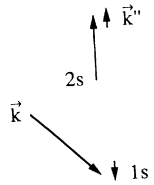

FIG. 9. Auger-deexcitation process with emission of spin-up electrons $N_{\uparrow}(E)$. The ejected electron is denoted $\mathbf{k}''$, the He ground state $1s$ and excited state $2s$, and $\mathbf{k}$ is a metal conduction-band electron.

same way as in Eqs. (1) and (2) as

$$N_{\downarrow}(E)=0 , \tag{24}$$

$$N_{\uparrow}(E)=\frac{2\pi}{\hbar}\sum_{\mathbf{k},\mathbf{k}''} f(k)|M^{\mathbf{k}2s}_{1s\mathbf{k}''}|^2\delta(E_{\mathbf{k}''}-E_{2s}+E_{1s}-E_{\mathbf{k}}) \times\delta(E_{\mathbf{k}''}-E) , \tag{25}$$

where M is the Coulomb matrix element. Taking the Fourier transform of the Coulomb interaction in the parallel direction, and using a classical surface response function in the same way as above, the matrix element can be expressed as in Eq. (6). However, the AD and RI processes both take place at larger distances from the surface than the AN process. We therefore simplify our calculation by not taking metal screening into account. We also assume that the ejected electrons are produced outside the surface, i.e., the overlap between $|2s\rangle$ and $|\mathbf{k}''\rangle$ is negligible inside the metal. For the metal state $|\mathbf{k}\rangle$ and the helium $|1s\rangle$ state, we use the same wave functions as described in Sec. II. The free-electron state $|\mathbf{k}''\rangle$ is also taken as a plane wave as before. For the excited helium state we use a Slater orbital. In this case, the exponential decay is characterized by λ_{2s} that is given by $0.58a_0^{-1}$ for the Slater $2s$ orbital in helium.[24] At relatively large distances ($\gtrsim 5$ Å) between the atom and the surface, the $2s$ orbital has been shown to be largely spherical with only a slight orientation toward the surface.[17] With decreasing distance to the surface, the width of the $2s$ state shows a nearly exponential increase. Close to the surface, however, hybridization has been shown to have a pronounced effect on RI and gives a saturation of the width.[17]

Since the purpose of this section is to get only a rough approximation of the AD and RI rates, we continue the calculation without taking screening and hybridization into account. The calculated AD rate as a function of the atom-surface distance d is shown in Fig. 4. As expected, the AD rate is much larger than the AN rate for specific distances outside the surface. We also notice a stronger dependence on the distance, i.e., a steeper slope, for the AN rate, as discussed in Sec. II. Because the slope has a strong influence on the most probable distance of transition, this assures that the AD process takes place further out from the surface than AN, as will be discussed in Sec. V.

In calculating RI, we use first-order perturbation theory. Treating the Coulomb interaction as the disturbance, the corresponding matrix element can be expressed as

$$M^{2s}_{\mathbf{k}}=\langle\mathbf{k}|(e^2/4\pi\epsilon_0 r)|2s\rangle . \tag{26}$$

We calculate, using the same wave functions as above but not taking screening into account, the RI rate as a function of the distance d between the atom and the surface. Figure 4 shows the RI rate together with the rates for AD and AN. The RI rate is larger than both the AD and the AN rate for specific distances outside the surface. However, the dependence of the distance for RI is similar to that for AD, since the corresponding matrix elements only contain one metal state. This assures that both the RI and AD processes take place further out from the surface than AN and that AD has the possibility to compete with RI.

In this section we have roughly estimated the production rates for electrons ejected from the AD and RI processes. We have to incorporate, as we show in the next section, at least three different processes in explaining the ejected electron distribution and polarization from metastable He-copper interaction. In our treatment we use the most probable distance for different processes to occur. In the next section we discuss the choice of a most probable distance from a set of rate equations and address the question of the number of ejected electrons from AD to explain the increase in the polarization at high energies in Fig. 1.

V. MOST PROBABLE DISTANCE FOR TRANSITIONS

We now turn to a discussion of the choice of most probable distances for AN and AD. From a set of rate equations together with the earlier calculated production rates, we derive approximations to the most probable distances where the AN, AD, and RI processes take place.

We start from the following rate equations to determine the relative number of excited helium atoms $n^*(z)$, helium ions $n^+(z)$, and ground-state helium atoms $n^0(z)$:

$$\frac{d}{dz}n^*(z)=-\frac{\tau_{RD}^{-1}(z)}{v^*}n^*(z) , \tag{27}$$

$$\frac{d}{dz}n^+(z)=-\frac{\tau_N^{-1}(z)}{v^+(z)}n^+(z)+\frac{\tau_R^{-1}(z)}{v^*}n^*(z) , \tag{28}$$

$$n^0(z)+n^*(z)+n^+(z)=1 , \tag{29}$$

where v^* is the velocity of the helium atoms and $v^+(z)$ is the velocity of the helium ions. τ_N^{-1}, τ_D^{-1}, and τ_R^{-1} are the transition rates for the AN, AD, and RI processes as calculated in Secs. II–IV, and $\tau_{RD}^{-1}\equiv\tau_R^{-1}+\tau_D^{-1}$. For large distances outside the surface $(z\rightarrow\infty)$, n^0 and n^+ are equal to zero, and n^* is equal to one. An ion is expected to feel its image charge and is therefore attracted to the surface with a resulting increase in velocity near the surface according to the relation

$$m_{\mathrm{He}}v^{+2}(z)/2=m_{\mathrm{He}}v^{*2}(\infty)/2+e^2/(16\pi\epsilon_0 z) ,$$

where m_{He} is the mass of helium.

To be able to calculate the most probable distance for the processes, we need to have accurate magnitudes of the transition rates. In our calculation of the AN, AD, and RI rates, we have approximated the metal wave func-

tions from the square barrier model, which are expected to underestimate the rates as compared to more elaborate jellium models. A more realistic barrier that includes the effect of the He is known to have a lower height.[7] An exponentially decaying wave function can still be used, but it has to be modified with a weakly energy-dependent decay factor and a more strongly energy-dependent shift of origin according to Eq. (30),[7]

$$|\phi_{k_\perp}(z)|^2 = e^{-a(\epsilon)[z - z_0(\epsilon)]}, \tag{30}$$

where $a(E_F) \approx 1.4$ Å^{-1} and $z_0(E_F) \approx 4$ Å. This modification was developed with an origin ($z=0$) at the jellium edge. In the infinite barrier model, the distance between the jellium edge and the potential step is $3\pi/(8k_F)$, which in our case is ≈ 0.8 Å. For the finite square barrier model this distance is smaller, ≈ 0.2 Å, which is small compared to the distance between the surface and the He. Therefore we consider Eq. (30) also to be valid in our case, where the origin is at the potential step. Although the modification of the wave function according to Eq. (30) depends on electron energy, we consider the electrons near the Fermi level to be most important in our processes. Within these assumptions, we notice that our origin at $z=0$ has to be moved approximately 3–4 Å outside the surface to give the correct transition rates.[7]

We notice that the energy-integrated transition rates in Fig. 4, as functions of the distance d between the helium and the surface, are characterized by their exponentially decaying behavior. Fitting such exponential functions helps us to solve Eqs. (27)–(29). The result, after taking the effect of a more accurate metal wave function according to Eq. (30) into account, is shown in Fig. 10. Relative numbers of excited helium atoms $n^*(z)$, helium ions $n^+(z)$, and ground-state helium atoms $n^0(z)$ are shown together with the filling probabilities $P_N(z) = [n^+(z)\tau_N^{-1}/v^+(z)]/P_{N\max}$, $P_D(z) = [n^*(z)\tau_D^{-1}/v^*]/P_{D\max}$, and $P_R(z) = [n^*(z)\tau_R^{-1}/v^*]/P_{R\max}$ for the AN, AD, and the RI processes. We notice that the most probable distance, i.e., the position of the maximum for the filling probabilities, for the RI and the AD processes lies around 7 Å. The most probable distance for AN is closer to the surface, approximately at 3 Å. From Fig. 4 we notice that at 7 Å the transition rate for the AD process is around 1–2 % of the transition rate for the RI process. Therefore a small fraction of the metastable helium atoms is deexcited through AD. This amount suffices, however, to explain the increase in Fig. 1 of the polarization at high energies, as discussed below.

The slope of the different transition rates in Fig. 4 is the main factor that determines the most probable distance of transition. AD and RI have similar slope, and these processes will therefore take place at almost the same distance. A much steeper slope for AN secures that AN takes place much closer to the surface, as illustrated in Fig. 10. The magnitudes of the rates at a given distance give the relative transition rates for the different processes. Using the most probable distance as representative for a whole process is a good approximation only if the filling probabilities are localized in space. We notice that the filling probabilities in Fig. 10 exhibit narrow peaks around specific distances. Therefore we consider the most probable distances to represent the processes well in our case.

Using the most probable distance as representative for the AN and AD processes, and taking the generation of secondary electrons from the AN process into account, we put the different processes together and show our calculated total ejected electron rate per energy interval and the polarization in Fig. 11. This should be compared

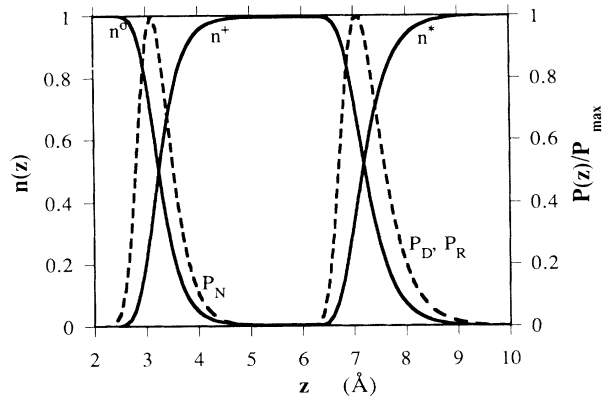

FIG. 10. Relative number of excited helium atoms $n^*(z)$, helium ions $n^+(z)$, and ground-state helium atoms $n^0(z)$ at different distances from the surface. Also shown are the filling probabilities $P_N(z) = [n^+(z)\tau_N^{-1}/v^+(z)]/P_{N\max}$, $P_D(z) = [n^*(z)\tau_D^{-1}/v^*]/P_{D\max}$, and $P_R(z) = [n^*(z)\tau_R^{-1}/v^*]/P_{R\max}$ at different distances for the AN, AD, and the RI processes. The filling probabilities are normalized to their maximum. $v^*(z)$ is the velocity of the helium atoms and $v^+(z)$ is the velocity of the helium ions. The transition rates τ^{-1} are taken from the calculations in Secs. II, III, and IV.

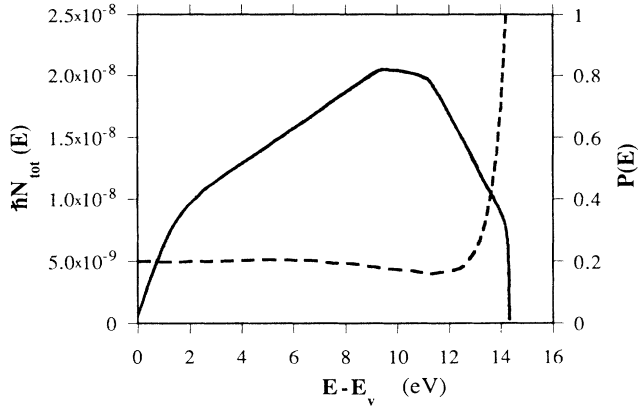

FIG. 11. Calculated total ejected electron distribution per energy interval $N_{\rm tot}(E) = N_\uparrow(E) + N_\downarrow(E)$ and spin polarization $P(E)$ (dashed line) from the Auger neutralization, secondary-electron, and Auger-deexcitation processes as a function of ejected electron energy. The calculation is done for a most probable distance of 3 Å between the helium ion and the metal surface for the Auger neutralization and secondary processes. Auger deexcitation is calculated for a most probable distance of 7 Å. E_v is the vacuum level. This figure should be compared with the experimental results in Fig. 1.

with the experimental results in Fig. 1. Only by incorporating all these three different processes in our theory do we manage to get a good agreement between theory and experiment. We discuss this further in the next section. Because AD contributes to a relatively small fraction of the ejected electrons and the electrons from AD originate from the He atom, we have not incorporated secondary electrons from the AD process in our calculations.

VI. SUMMARY AND CONCLUSIONS

In this paper we have treated electrons emitted in spin-polarized metastable He-metal (Cu) interaction. We can only explain the experimentally emitted electron distribution and spin polarization in Fig. 1 if we incorporate three different processes: Auger neutralization (AN), secondary electrons, and Auger deexcitation (AD).

The main contribution to the ejected electron distribution comes from the AN process. We start from the golden rule, using simple wave functions and taking metal screening into account, to calculate the AN transition rate. The region between the surface and the He is found to be of great importance in calculating the transition rate. As a consequence, we consider *d*-band electrons to be of less importance in AN. AN with its exchange matrix element is also found to be the main source of spin polarization. A SPMDS experiment on a nonmagnetic material therefore directly measures the exchange scattering. We estimate that the AN process occurs at a most probable distance of around 3 Å outside the surface. However, AN does not explain the ejected electron distribution and polarization at the lowest and highest energies. Therefore we consider other possible processes to be important at these energies.

In the lowest energy range, secondary-electron processes from AN are the major source of generating almost unpolarized electrons. Starting from the Boltzmann transport equation, using a simple kernel that fulfills a sum rule associated with the production of secondary electrons, we calculate the secondary-electron contribution to the AN process. In the energy region of interest, electrons are known to have rather long mean free paths (5–10 Å) compared to the size of the surface region (limited by the He extension) where the AN process takes place. The electrons can then move large distances without generating electron-hole pairs, and they have a large probability, determined by the surface transmission function, to escape from the solid. Therefore we expect only the first few generations of secondary electrons to be of importance. Within this model, secondary electrons give a significant contribution to the AN process in the low-energy range and the calculated ejected electron distribution in Fig. 7 is in good agreement with the experimental cross section. Secondary electrons also manage to bring down the high polarization of AN. AN with associated secondary electrons give an almost constant spin polarization of around 20% if we, as a representative for the AN process within the square barrier model, use a most probable distance of 3 Å.

In the high-energy range, we consider ejected electrons from the AD process (100% spin polarization) to be the source of a measured increasing spin polarization. When excited He atoms move toward the surface, AD competes with resonant ionization (RI). We estimate the RI rate from first-order perturbation theory and compare it with AD, which is calculated, without taking metal screening into account, from the golden rule. AD explains the experimentally measured high polarization at the highest energies for a most probable distance of around 7 Å. All rates as functions of the distance to the surface exhibit almost exponentially decaying behaviors. However, close to the surface ($\lesssim 3$ Å) the rates are known to saturate.[17] Our model does not, however, take such saturation into account. Both the calculated RI and AD rates are greater than the AN rate for specific distances. RI and AD therefore have the possibility to take place further out from the surface than AN. Comparing the transition rates with each other reveals that around 2% of the ejected electrons originate from the AD process. This amount suffices to explain the measured increase in polarization at the highest energies. Taking all the above-described processes into account, the calculated ejected electron distribution and polarization are shown in Fig. 11 and should be compared with Fig. 1.

We notice that the filling probabilities for the AN, RI, and AD processes in Fig. 10 exhibit narrow peaks around specific distances. This leads us to the conclusion that the choice of a most probable distance represents the different processes well in our case. When the incoming excited He atoms reaches around 7 Å outside the surface, it undergoes a transition to an ion. This ion survives to a distance of around 3 Å, where it is neutralized to a ground-state He atom. The incoming He therefore goes through three different stages that are spatially rather well defined.

Metal screening turns out to be important in the AN process. We take both an ω and $\mathbf{k}$ dependence of the screening into account by introducing a surface response function $\epsilon(\mathbf{k}_{\parallel},\omega)$. Screening increases the AN rate with approximately a factor of 2. This condition of antiscreening has its origin from the values of $\epsilon(\mathbf{k}_{\parallel},\omega)$ in the particular energy range under consideration. We note that more important than screening is the use of proper metal wave functions that take into account the lowering of the surface barrier as the He ion approaches the surface.

For the future, we find it important to incorporate more accurate wave functions to be able to calculate the magnitude of the transition rates better. Also a proper orthogonalization is needed to treat the singularity in $\mathbf{k}$ space. Instead of using the most probable distances for the various processes, we could integrate over the trajectory of the incoming He. However, our results give a good agreement with the measurement, and we therefore consider the most probable distances to be good representatives for the processes. The velocity of the incoming He has so far been neglected in the matrix elements. It would be interesting to study to what extent a finite velocity of the incoming He affects the transition rates and the polarization. This should be of particular importance for calculating transition rates and most probable distances for the transitions. Also, the position of the most

probable distances, and the regions of different stages of the He, as discussed above, may be altered by changing the incoming velocity. The recently reported saturation of width of states very near the surface can have a significant effect on the transition rates.[17] This should not only be true for AD, as reported, but also for AN with its most probable distance closer to the surface than AD.

ACKNOWLEDGMENTS

We thank P. Apell, C. Monreal, F. Flores, T. Fondén, A. Zwartkruis, P. Echenique, and D. Penn for many useful discussions. This project was supported by the Swedish Natural Science Research Council.

APPENDIX

In this appendix, we follow the treatment in Ref. 25 to derive the expression used in Sec. II for introducing a wave-vector dependence in the classical surface response function. We study the problem by defining symmetrized extended pseudomedia, whose definition includes a fictitious surface charge distribution. The surface charge is later eliminated by imposing matching conditions. Consider a moving point charge outside ($z>0$) an infinite metal surface. A moving point charge with velocity $\mathbf{v}$ can be described as

$$\rho^{\text{ext}}(\mathbf{r},t)=Q\delta(\mathbf{r}-\mathbf{v}t)\ , \tag{A1}$$

where we set $Q=1$ for simplicity. Fourier transforming this charge distribution and solving the Poisson equation within the extended pseudomedia scheme gives the total potential in the extended pseudovacuum (denoted 1) from the moving point charge and the response from the metal as

$$\phi^{(1)}(\mathbf{k},\omega)=\frac{8\pi^2}{k^2}[\delta(\omega-\mathbf{k}\cdot\mathbf{v})+\delta(\omega-\mathbf{k}\cdot\mathbf{v}')+\sigma(\mathbf{k}_\parallel,\omega)]\ , \quad z>0\ . \tag{A2}$$

$\mathbf{v}'$ is the velocity of the image point charge and σ is the fictitious induced charge distribution at the metal surface, which we later will eliminate. In the extended pseudomedium (denoted 2) the potential can be expressed as

$$\phi^{(2)}(\mathbf{k},\omega)=-8\pi^2\frac{\sigma(\mathbf{k}_\parallel,\omega)}{k^2\epsilon(\mathbf{k}_\parallel,\omega)},\quad z<0\ . \tag{A3}$$

Matching Eqs. (A2) and (A3) at the surface ($z=0$) gives the fictitious surface charge distribution σ as

$$\sigma(\mathbf{k}_\parallel,\omega)=-\frac{\int\frac{dk_\perp}{k^2}[\delta(\omega-\mathbf{k}\cdot\mathbf{v})+\delta(\omega-\mathbf{k}\cdot\mathbf{v}')]}{\frac{\pi}{k_\parallel}+\int\frac{dk_\perp}{k^2}\frac{1}{\epsilon(\mathbf{k}_\parallel,k_\perp,\omega)}}\ . \tag{A4}$$

Substituting Eq. (A4) into Eq. (A2) gives the induced charge distribution ϕ^{ind} outside the metal as

$$\phi^{\text{ind}}(\mathbf{k},\omega)=\phi^{(1)}(\mathbf{k},\omega)-\phi^{\text{ext}}(\mathbf{k},\omega)=\frac{8\pi^2}{k^2}\left[\delta(\omega-\mathbf{k}\cdot\mathbf{v}')-\frac{\int\frac{dk_\perp}{k^2}[\delta(\omega-\mathbf{k}\cdot\mathbf{v})+\delta(\omega-\mathbf{k}\cdot\mathbf{v}')]}{\frac{\pi}{k_\parallel}+\int\frac{dk_\perp}{k^2}\frac{1}{\epsilon(\mathbf{k}_\parallel,k_\perp,\omega)}}\right]\ . \tag{A5}$$

We now Fourier transform Eq. (A5) back to $(\mathbf{r},t)$ space and get

$$\phi^{\text{ind}}(\mathbf{r},t)=\int\frac{d\mathbf{k}_\parallel}{2\pi^2}d\omega\frac{|v_\perp|}{k_\parallel^2\mathbf{v}_\perp^2+(\omega-\mathbf{k}_\parallel\cdot\mathbf{v}_\parallel)^2}\times e^{-k_\parallel z}e^{i(\mathbf{k}_\parallel\cdot\mathbf{r}_\parallel-\omega t)}\left[1-\frac{2}{B(\mathbf{k}_\parallel,\omega)}\right]\ , \tag{A6}$$

where $v_\perp$ is the velocity perpendicular to the surface and $B(\mathbf{k}_\parallel,\omega)$ is defined as

$$B(\mathbf{k}_\parallel,\omega)\equiv 1+\frac{k_\parallel}{\pi}\int\frac{dk'_\perp}{k_\parallel^2+k_\perp'^2}\frac{1}{\epsilon(\mathbf{k}_\parallel,k'_\perp,\omega)}\ . \tag{A7}$$

The potential from the external point charge in Eq. (A1) can be expressed as in Eq. (A8):

$$\phi^{\text{ext}}(\mathbf{r},t)=\int\frac{d\mathbf{k}_\parallel}{2\pi^2}d\omega\frac{|v_\perp|}{k_\parallel^2v_\perp^2+(\omega-\mathbf{k}_\parallel\cdot\mathbf{v}_\parallel)^2}e^{k_\parallel z}e^{i(\mathbf{k}_\parallel\cdot\mathbf{r}_\parallel-\omega t)}\ . \tag{A8}$$

In the region outside the surface, the total potential is a contribution from the external point charge and the response from the metal. We therefore arrive at the following expression for the total potential outside the surface:

$$\phi(\mathbf{r},t)=\int\frac{d\mathbf{k}_\parallel}{2\pi^2}d\omega\frac{|v_\perp|}{k_\parallel^2v_\perp^2+(\omega-\mathbf{k}_\parallel\cdot\mathbf{v}_\parallel)^2}e^{i(\mathbf{k}_\parallel\cdot\mathbf{r}_\parallel-\omega t)}\times\left[e^{k_\parallel z}+\left[1-\frac{2}{B(\mathbf{k}_\parallel,\omega)}\right]e^{-k_\parallel z}\right]\ . \tag{A9}$$

A comparison between Eq. (A9) and the classical surface response function $g(\omega)=[\epsilon(\omega)-1]/[\epsilon(\omega)+1]$ (see Ref. 12), where ϵ is the dielectric function, gives that the classical surface response function $g(\omega)$ here corresponds to $2/B(\mathbf{k}_\parallel,\omega)-1$. Now we introduce a wave-vector dependence into the classical surface response function through the exchange of $g(\omega)$ with

$$\frac{2}{B(\mathbf{k}_\parallel,\omega)}-1=\frac{1-\frac{k_\parallel}{\pi}\int\frac{dk'_\perp}{k_\parallel^2+k_\perp'^2}\frac{1}{\epsilon(\mathbf{k}_\parallel,k'_\perp,\omega)}}{1+\frac{k_\parallel}{\pi}\int\frac{dk'_\perp}{k_\parallel^2+k_\perp'^2}\frac{1}{\epsilon(\mathbf{k}_\parallel,k'_\perp,\omega)}}, \quad \text{(A10)}$$

which is the same as if we in the classical expression $g(\omega)=[\epsilon(\omega)-1]/[\epsilon(\omega)+1]$ exchange $1/\epsilon(\omega)$ according to

$$\frac{1}{\epsilon(\omega)}\rightarrow\frac{1}{\epsilon(\mathbf{k}_\parallel,\omega)}\equiv\frac{k_\parallel}{\pi}\int\frac{dk_\perp}{k_\parallel^2+k_\perp^2}\frac{1}{\epsilon(\mathbf{k}_\parallel,k_\perp,\omega)}. \quad \text{(A11)}$$

[1]J. Kirschner, D. Rebenstorff, and H. Ibach, Phys. Rev. Lett. **53**, 698 (1984).

[2]J. Glazer and E. Tosatti, Solid State Commun. **52**, 905 (1984).

[3]H. Hopster, R. Raue, and R. Clauberg, Phys. Rev. Lett. **53**, 695 (1984).

[4]H. R. Moser and G. Wendin, Solid State Commun. **65**, 107 (1988).

[5]D. Venus and J. Kirschner, Phys. Rev. B **37**, 2199 (1988).

[6]M. W. Hart, M. S. Hammond, F. B. Dunning, and G. K. Walters, Phys. Rev. B **39**, 5488 (1989).

[7]D. R. Penn and P. Apell, Phys. Rev. B **41**, 3303 (1990).

[8]H. D. Hagstrum, Phys. Rev. **96**, 336 (1954).

[9]S. Horiguchi, K. Koyama, and Y. H. Ohtsuki, Phys. Status Solidi B **87**, 757 (1978).

[10]R. Hentschke, K. J. Snowdon, P. Hertrel, and W. Heiland, Surf. Sci. **173**, 565 (1986).

[11]V. L. Moruzzi, J. F. Janak, and A. R. Williams, *Calculated Electronic Properties of Metals* (Pergamon, New York, 1978).

[12]B. N. J. Persson and E. Zaremba, Phys. Rev. B **31**, 1863 (1985).

[13]See, e.g., J. J. Sakurai, *Modern Quantum Mechanics* (Benjamin/Cummings, Menlo Park, 1985).

[14]H. D. Hagstrum, Phys. Rev. **150**, 495 (1966).

[15]H. D. Hagstrum and G. E. Becker, Phys. Rev. **159**, 572 (1967).

[16]A. Zangwill, *Physics at Surfaces* (Cambridge University Press, Cambridge, 1988).

[17]F. B. Dunning, P. Nordlander, and G. K. Walters, Phys. Rev. B **44**, 3246 (1991).

[18]F. García-Moliner and F. Flores, *Introduction to the Theory of Solid Surfaces* (Cambridge University Press, Cambridge, 1979).

[19]H. J. Hagemann, W. Gudat, and C. Kunz, J. Opt. Soc. Am. **65**, 742 (1975).

[20]R. K. Janev and N. N. Nedeljkovic, J. Phys. B **18**, 915 (1985).

[21]P. A. Wolff, Phys. Rev. **95**, 56 (1954).

[22]D. R. Penn, S. P. Apell, and S. M. Girvin, Phys. Rev. B **32**, 7753 (1985).

[23]D. R. Penn, Phys. Rev. B **35**, 482 (1987).

[24]E. Clementi and C. Roetti, At. Data Nucl. Data Tables **14**, 177 (1974).

[25]F. Flores and F. García-Moliner, J. Phys. C **12**, 907 (1979).